Wiener filtering with a seismic underground array at the Sanford Underground Research Facility

M Coughlin

Department of Physics, Harvard University, Cambridge, MA 02138, USA

J Harms

INFN, Sezione di Firenze, Firenze 50019, Italy

N Christensen

Physics and Astronomy, Carleton College, Northfield, Minnesota 55057, USA

V Dergachev

LIGO Laboratory, California Institute of Technology,

MS 100-36, Pasadena, CA, 91125, USA

R DeSalvo

Collegio di Dottorato, University of Sannio, Benevento 82100, Italy

S Kandhasamy

Physics and Astronomy, University of Mississippi, University, MS 38677-1848, USA

V Mandic

School of Physics and Astronomy, University of Minnesota,

Minneapolis, Minnesota 55455, USA

arXiv:1403.7756v1 [gr-qc] 30 Mar 2014

Abstract

A seismic array has been deployed at the Sanford Underground Research Facility in the former Homestake mine, South Dakota, to study the underground seismic environment. This includes exploring the advantages of constructing a third-generation gravitational-wave detector underground. A major noise source would be Newtonian noise, which is induced by fluctuations in the local gravitational field. The hope is that a combination of a low-noise seismic environment and coherent noise subtraction using seismometers in the vicinity of the detector could suppress the Newtonian noise to required levels. In this paper, we use Wiener filtering techniques to subtract coherent noise in a seismic array in the form of oceanic microseisms. We achieve more than an order of magnitude noise cancellation between about 0.05-0.5 Hz. We examine the variation in the Wiener filter coefficients over the course of the day, showing how local activities impact the filter. We also study the variation in coefficients over the course of a month, showing the stability of the filter with time. We finally explore how varying the filter order affects the subtraction performance. It is shown that optimizing filter order can significantly improve subtraction performance.

I. INTRODUCTION

In the following years, a second generation of laser-interferometric gravitational-wave (GW) detectors will start operating with the goal to directly observe GWs produced for example by supernovae, or the merger of neutron stars and black holes. The global network of detectors will consist of the two Advanced LIGO [1] interferometers in Louisiana and Washington State, US, the Advanced Virgo [2] interferometer near Pisa, Italy, and the KAGRA interferometer at the Kamioka mine in Japan [3]. Gravitational waves produce changes in distance between test masses smaller than 10^{-20} m, which will be observed by these detectors. Isolating test masses in gravitational-wave detectors from seismic disturbances is one of the foremost challenges of the instrumental design. Second-generation detectors will use sophisticated seismic-isolation systems to make possible the detection of GWs above 10 Hz. For this purpose, the isolation systems consist of chains of coupled springs and pendulums with lowest resonance frequencies around 1 Hz so that seismic noise well above these frequencies is suppressed by many orders of magnitude in all rotational and translational degrees of freedom. The goal of future detectors, such as the Einstein Telescope (ET) [4], will be to extend the detection band to even lower frequencies. This poses an even greater challenge to the design of the isolation system.

The mechanical, or passive, component of the isolation system is assisted by a complex network of sensors and actuators forming the so-called active seismic isolation [5]. Sensor data recorded on some of the mechanical stages of the passive system are used to calculate a feedback force acting on the mechanical stage to suppress seismic disturbances. Another variant of the active isolation scheme is the feed-forward noise cancellation [6–8]. For example, data from a seismic sensor deployed directly on the ground close to a test mass can be used to cancel seismic noise further down the isolation chain, provided that there is residual correlation between motion of the ground and of some part of the isolation system. Under ideal conditions, the limit of what can be achieved with the active system is determined by the sensitivity of the seismic sensors.

Seismic disturbances can also affect test-mass motion via gravitational coupling circumventing the entire seismic isolation system [9–11]. This so-called Newtonian noise (NN) has never been observed, but it is predicted to be one of the limiting noise sources in advanced detectors at frequencies between 10 Hz and 20 Hz. As it is impossible to shield a test mass

from NN, another method needs to be found to suppress it. One possibility, at least for future detectors, is to select a site that shows very low levels of seismic noise [12, 13]. The construction of underground detectors has been proposed for this purpose [4]. However, this option is costly, and does not apply to any of the existing surface sites of the LIGO and Virgo detectors. Another idea is to attempt a feed-forward noise cancellation using auxiliary sensors [14]. For example, gravity perturbations caused by seismic fields can be estimated in real time using data from an array of seismic sensors [15].

For stationary, linear systems, the optimal filter used for a feed-forward noise cancellation is the Wiener filter [16]. It is calculated from correlations between data of the auxiliary sensors and data observed at the target point where noise is to be suppressed. The parameters of the optimal linear filter under ideal conditions are fully determined by the data correlations and the frequency range over which noise cancellation is to be achieved. In reality though, as will be shown in the following, filter parameters can be further optimized to account for non-stationary properties of the data and variations of the dynamics of the system; one possible example is temperature drift. With respect to slow changes in noise variance or system dynamics, one can simply update the Wiener filter regularly using the latest observed data or implement an adaptive filter technology [17]. However, as will be shown in this paper, in the presence of non-stationary seismic noise, improvement can also be achieved by optimizing the number of filter coefficients. This parameter is a constant in all adaptive filter schemes known to the authors.

Wiener filtering with seismic arrays has been performed in the past to improve signal-to-noise ratios towards weak seismic signals [18]. In this paper, we present results from a study of feed-forward noise cancellation by means of Wiener filters calculated from correlations between seismic sensors of an underground array. The seismic sensors are broadband instruments sensitive to seismic noise between about 10 mHz and 50 Hz. The array is located at the Sanford Underground Research Facility in the Black Hills of South Dakota [13]. Three stations with good data quality were active during this study using data from February and March 2012: one at 800 ft depth, one at 2000 ft, and one at 4100 ft. The focus lies on the subtraction of oceanic microseisms observed below 1 Hz. The Wiener filters are realized as finite-impulse response (FIR) filters. The two main parameters investigated here are the rate at which the filters are updated, and the number of filter coefficients.

A brief summary on data quality issues in gravitational-wave detectors in general, and

specifically of the seismic data used in this study is given in section II. In section III, the Wiener filtering method used in this work is described. The results are given in section IV, and our conclusions are summarized in section V.

II. DATA QUALITY

There are two major types of data quality issues in laser-interferometric gravitational wave detector data: spectral lines and glitches. Lines due to noise usually occur at well defined frequencies in detector data (though some of these lines are broad and others wander) [19, 20]. Signals can be introduced by computer clocks, periodic radio transmissions, and other digitized signals from the equipment monitoring the detector. Periodic environmentally triggered signals such as pumps or cooling fans, vibrational modes of the suspension systems, and line noise due to the power supplies are other possible sources. Anthropogenically produced noise sources are known to have broader spectra and to wander in frequency, so these will be particularly harmful.

Despite the fact that the optical system is constructed in vacuum, and the test masses are suspended from seismically isolated platforms, detectors are susceptible to a variety of instrumental and environmental noise sources that decrease their detection sensitivity [21, 22]. Short in duration, non-astrophysical transient events or *glitches* can mask or mimic real signals. Environmental noise can couple into the interferometer through mechanical vibration or because of magnetic fields which can produce forces on magnets in the suspension systems. Seismic motion from human activity near the sites, from wind, and from ocean waves are among the most common sources of these disturbances. It is important for filtering methods to be robust against such artifacts, as blindly applying a filter with inputs affected by transients could introduce noise into the target channel. Meadors et al. [23] successfully applied a subtraction algorithm, based on Allen, Hua, and Ottewill's frequency domain transfer function fitting [24] to data from LIGO's S6 science run to increase strain sensitivity. To overcome the transients issue, they only applied the algorithm when the subtraction improved the sensitivity.

In this paper, the reference and target data will come from seismometers of an underground array. Below 1 Hz, the seismic spectrum is dominated by the primary and secondary microseismic peaks. Far from the ocean, microseisms appear with approximately the same

amplitude both above and below ground. These occur between 30 – 100 mHz, and 0.1 – 0.5 Hz respectively. This is the main source of coherent noise we seek to subtract. A potential local source of low-frequency seismic disturbances is wind. However, a previous study indicated that at stations at depths of 800 ft or more, correlation between seismicity and wind speeds is insignificant (while the effect was significant at 300 ft) [13], implying a relatively short correlation length of the respective seismic disturbance. The strongest sources of low-frequency noise are earthquakes. The closest or highest magnitude events can also significantly contribute to seismic motion above 1 Hz. Above 1 Hz, previous work identified the mine as a world-class low-noise environment [13].

III. WIENER FILTERING

In the following, we will describe feed-forward noise cancellation using seismic data. It should be mentioned though that this is not the only conceivable application of feed-forward noise cancellation in interferometers (see for example [25]). When creating a feed-forward filter to subtract seismically induced noise in GW detectors, the target point can either be located within the seismic isolation chain monitored by a seismic sensor, or it can be the test mass or other optics whose positions are read out interferometrically. The reference sensors used as filter inputs typically include seismometers surrounding the respective optics [7, 15]. Since there are in general several input sensors and one target point, the filter configuration is also known as multiple-input, single output (MISO). The goal is to design a MISO filter that combines the data from all seismometers to produce an optimal estimate of the motion of the target point. This allows removal of seismic noise coupled to the detector data, including NN, without a priori assumptions about the modal content and directionality of the seismic waves. Instead, the filter is derived solely from the input and output data via the filter optimization process.

The type of MISO filter produced depends on the type of noise. If the noise is modelled as a statistically stationary process (one whose parameters are constant in time), the optimal filter is constant in time. Then, the filter is only created once and thereafter can be applied to the data continuously. These types of filters satisfy the Wiener-Hopf equations and are known as *Wiener filters* [16]. The simplest kind of Wiener filter to implement is a causal Finite Impulse Response (FIR) Wiener filter, which is characterized by a vector of real

numbers that represent an impulse response. This vector is convolved with the input signal in the time domain to obtain the optimal estimate of the noise.

The basic principle of Wiener filters is to use the output of a number of reference traces to predict the noise of a target channel. This prediction is then subtracted from the target channel, typically in real time, leaving the non-correlated residual. Given the input time series $\vec{x}(k) = (x_m(k))$ with $m = 1, \ldots, M$ from M reference channels, and output time series $y(k)$ from a single target channel, we desire to create an FIR filter with $L + 1$ coefficients $\vec{f}(l) = (f_m(l))$, $l = 0, \ldots, L$ that minimizes the residual error:

$$E = \sum_{k=1}^{N} \left(y(k) - \sum_{l=0}^{L} \vec{f}(l) \cdot \vec{x}(k-l) \right)^2 \tag{1}$$

where N is the number of samples. Each coefficient of the optimal filter must obey

$$\frac{\delta E}{\delta f_m(l)} = 0 \tag{2}$$

This constraint results in

$$\sum_{l=0}^{L} R_{xx}(k-l) \cdot \vec{f}(l) = \vec{c}_{yx}(k) \tag{3}$$

where R_{xx} is the auto-correlation of $\vec{x}$, $\vec{c}_{yx}$ is the cross-correlation between y and $\vec{x}$, and $k \in 0, \ldots, L$. Equation (3) is known as the Wiener-Hopf equation, which represents a series of $(L + 1)M$ equations for the same number of optimal filter coefficients $f_m(l)$ that must be solved simultaneously. Because the signals are real, their autocorrelation is symmetric, $R_{xx}(k) = R_{xx}(-k)$, resulting in a Toeplitz structure for the system of equations, which makes it possible to apply more efficient algorithms when solving for the filter coefficients. The noise cancellation algorithm can then be written symbolically as a convolution (symbol $*$) [16]:

$$r(k) = y(k) - \sum_{m=1}^{M} (f_m * x_m)(k) \tag{4}$$

If the noise-cancellation filter is meant to perform best during times without major seismic disturbances such as earthquakes, then one needs to make sure that the data used to calculate the filter coefficients are representative of quiet times. Equation (3) shows that the optimal filter coefficient depends on the average correlation between channels, but also on the spectra of all channels (otherwise optimal subtraction could be achieved with a single FIR filter coefficient per input channel). These changes can be related to specific properties of the seismic wave during strong ground motion, such as propagation direction, or wave content

(surface waves, body waves, polarization, etc). The spectrum of a seismic disturbance is typically determined by and therefore characteristic of its source. The typical situation however will be that the seismic field recorded over some time is composed of many seismic waves from different sources, and the Wiener filter calculated from it will by determined by the average correlations between channels and their average spectra.

It should be noted that coherence between channels needs to be very high even for "modest" noise cancellation. The ideal suppression factor $r(f)$ as a function of frequency f in the case of a single reference channel is related to the reference-target coherence $c(f)$ via

$$r(f) = \frac{1}{\sqrt{1 - c(f)^2}} \tag{5}$$

For example, if coherence between reference and target channels at some frequency is (0.9, 0.99, 0.999), then the residual amplitude spectrum at that frequency will ideally be reduced by factors (2.3, 7.1, 22) respectively. Therefore, a seismic noise reduction by a factor 50 is very impressive and requires a channel coherence of about 0.9998. As shown in section IV B, this suppression factor can be achieved, but since two reference channels are used in this study, one cannot translate this suppression into a value of two-point seismic coherence. A two-point coherence value of 0.9998 would also lie *above* the theoretical expectation (about 0.999) at least for an isotropic Rayleigh field (see for example equation (7) in [15]).

IV. FILTER RESULTS

Table I shows the locations of the seismometers used for our study at the 800 ft, 2000 ft-B, and 4100 ft-A stations. The horizontal distances between them are 800 ft/2000 ft-B = 295 m, 800 ft/4100 ft-A = 517 m, and 2000 ft-B/4100 ft-A = 790 m, and the total distances are 800 ft/2000 ft-B = 503 m, 800 ft/4100 ft-A = 1236 m, and 2000 ft-B/4100 ft-A = 1065 m. The horizontal distances are relevant to estimate coherence from seismic surface fields between stations, whereas the total distances are relevant to estimate coherence from body-wave fields. Coherence between channels is what fully determines the Wiener filter coefficients. Coherence is a consequence of the seismometer self noise, but also of the local geophysical settings and properties of the seismic field. Whereas the hard rock of the Black Hills should be beneficial to seismic coherence between stations as seismic waves are relatively long, topographic scattering, especially in mountainous regions, may pose an ultimate limit to

Station	Seismometer	Position (E,N) (m)
800 ft	T240	(-88,124)
2000 ft-B	T240	(-234,380)
4100 ft-A	STS-2	(347,-155)

TABLE I: Table detailing station information, including station names, type of seismometer, and position relative to Yates shaft of the former Homestake mine. For more details on the mine and available stations, please see [13]. T240 stands for Nanometrics Trillium 240 Broadband Sensor, and STS-2 stands for Streckeisen STS-2 Broadband Sensor.

what can be achieved with Wiener filtering irrespective of the sensor self noise [26]. Another limit of subtraction performance could be related to a complex composition of the seismic field. With the few seismometers that were used in this study, the Wiener filter is likely not able to subtract ambient noise from body waves to the same degree as the noise from the dominant Rayleigh waves. The latter is not obvious though, and needs to be investigated in the future using extended underground arrays. The basic idea is that a Wiener filter can only train on an average correlation pattern of a seismic array. The sign of average seismic correlation between two seismometers can be different for body and surface waves depending on the distance between them. This leads to partial cancellation of their contribution and affecting subtraction performance. However, if a seismic array is designed to have the ability to distinguish between body and surface fields, then also the Wiener filter will be able to subtract contributions from both.

Figure 1 demonstrates the performance of the filter on the seismic array data. A Wiener filter with 1000 coefficients was calculated from 3 hours of data, and then subsequently applied to subtract ambient seismic noise from target channels over a period of 2 weeks. In all cases, only the vertical channels were used as target and reference. Adding horizontal channels to the reference channels does not lead to significant changes of the subtraction residuals since coherence between horizontal and vertical directions is small. For target seismometers 800 ft and 2000 ft-B, subtraction residuals are more than a factor 10 weaker than the original spectra over a wide range of frequencies. Subtraction performance is significantly worse at 4100 ft-A. None of the geophysical effects outlined at the beginning of this section can explain this result. Therefore, we conclude that the 4100 ft-A seismometer

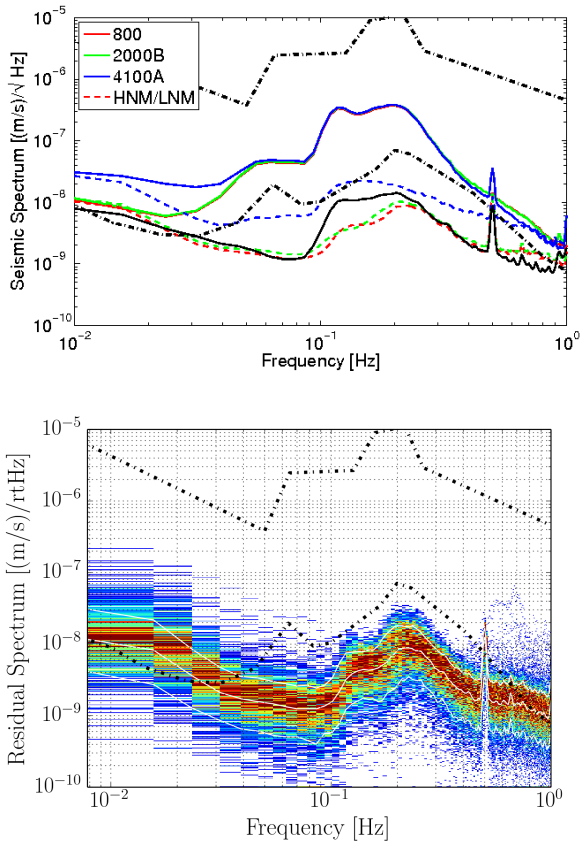

FIG. 1: The plot to the left shows the medians of seismic spectra (solid lines) for the three seismometers, and the medians of the residuals (dashed lines). For each dashed line, the vertical channel of the respective seismometer was the target channel, and channels from the other two sensors were used as reference channels. The dash-dotted lines in black represent the global low- and high-noise models [27]. The primary and secondary microseismic peaks are visible between 30 and 100 mHz and 0.1-0.5 Hz respectively. The expected subtraction for the 800 ft channel based on coherence between the 800 ft and 2000 ft-B stations is plotted in solid black. On the right is the full spectral histogram of the residual noise with 2000 ft-B target station, together with its 10th, 50th, and 90th percentiles.

must have an elevated noise floor, maybe because of problems with the data-acquisition system. Nevertheless, it is interesting that in all cases a residual microseismic peak (probably two peaks generated by two different ocean-wave fields) remains in the residual spectrum, and that this peak is larger than what is expected from an estimate of the Rayleigh wavelength (more than 10 km) in comparison to the horizontal station distance. This can be due to

a geophysical effect, but potentially also because of a weakly non-linear response of the seismometer.

The measured coherence between two stations can be used to calculate the spectrum of the uncorrelated seismic noise. The result is shown as black solid line on the left of figure 1 for the 800 ft – 2000 ft-B seismometer pair. As can be seen, the residual spectrum of the Wiener filter lies below the coherence limit, which means that even with one additional reference seismometer significant extra information about the seismic field can be obtained to improve noise cancellation. It is to be expected that a larger array with greater variation in station distances would yield even better subtraction over a broader range of frequencies, potentially down to the instrumental noise limit.

In general, Wiener filters introduce uncorrelated noise from the reference channels, which either contributes to the limit to how much noise suppression can be achieved, or even introduce excess noise in low-coherence bands if numerical problems at the filter training lead to sub-optimal filters (e. g. due to complex spectral shapes of the noise or a (too) high filter order). In the latter case, additional filters may be required to minimize noise introduced in the low-coherence band. In this study however, correlation between seismometers is significant below 1 Hz and only weak noise from the 4100 ft-A seismometer above about 0.5 Hz where the subtraction residuals lie above the coherence limits as shown in figure 1.

A. Filter evolution with time

Slow changes of average properties of the seismic field (e. g. diurnal or seasonal cycles), of instrumental noise, or of the system dynamics may require filter adaptation. When implementing a Wiener filter, it is important to know how often such a filter should be updated, or in case that the required update rate is high, if a genuine adaptive filter technology needs to be implemented. We now study how the filter coefficients evolve over time by recalculating the Wiener filter regularly.

We begin by examining filter evolution on day-long timescales by computing a filter every 128 s. An update scheme this fast is certainly not meant to be used in real applications and only serves to illustrate filter variations. The target seismometer is at the 800 ft station. Figure 2 shows the evolution of the Wiener filter over the course of a day. Results are given only for the part of the filter mapping the 2000 ft-B reference channel. Instead of directly

showing the FIR coefficients, the filter is represented in the frequency domain to make it easier to connect its variation with properties of the seismic field.

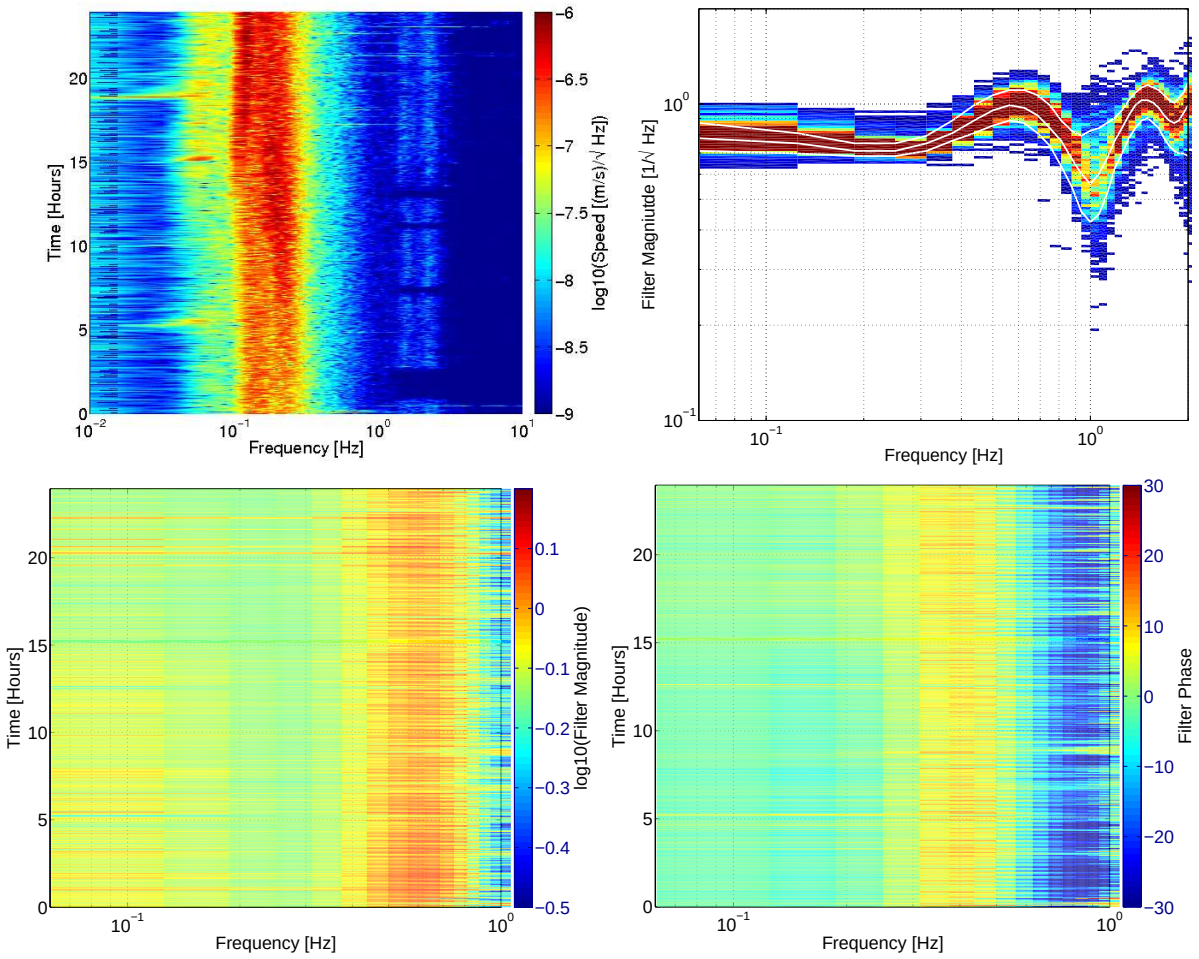

FIG. 2: Filter variation over the course of a day. Filter is represented in frequency domain by its magnitude and phase, as in a Bode plot. Top left: Time-frequency plot of the 800 ft seismometer. Top right: Filter magnitude histogram for the 2000 ft-B reference channel. Bottom left: Time-frequency plot of the filter magnitude for the 2000 ft-B reference channel. Bottom right: Time-frequency plot of the filter phase for the 2000 ft-B reference channel.

.

The fluctuations in the seismic spectra predominantly result in changes in the high frequency portion of the filter. The major variations in this portion coincide with high amplitude events in the seismic spectra. Due to its high frequency, this noise is likely local and therefore anthropogenic in origin. The histogram of filter magnitude variations is shown in

the top right plot. The distribution widens at high frequency, while it is narrowest around the oceanic microseisms. This is consistent with the fact that oceanic microseisms are stationary over the course of a day, whereas local noise below and above the microseismic peak is strongly non-stationary. It is maybe surprising that the low-frequency part of the filter does not vary as much as the seismic field itself, but important are variations of correlation between all channels. In the case of high correlation between channels during quiet time as is the case at lower frequencies, the effect of strong ground motion on correlation would simply be to increase correlation from say 0.9 to 0.95, which means that also the filter response should be expected to vary accordingly. Correlation is however small at higher frequencies during quiet times, and is increased significantly by strong ground motion, which would lead to large changes in the Wiener filter.

Because the spectral densities of all three channels involved in the noise subtraction are almost identical in the frequency range 0.1 Hz – 0.5 Hz, the fact that filter magnitudes for the 2000 ft-B are smaller than 1 in this frequency range means that the 4100 ft-A reference channel provides the missing part required for subtraction. The 4100 ft-A contribution is smaller due to the elevated instrumental noise of its seismometer. The filter magnitudes greater than 1 around 0.8 Hz are also expected because the target channel is closer to the surface and therefore has a significantly greater Rayleigh-wave amplitude at sufficiently high frequencies. Filter magnitude goes to zero at frequencies where coherence is weak, and the optimal filter suppresses incoherent noise contribution of the reference channel to the target channel.

Next we study how the filter evolves on month-long timescales. Figure 3 shows the 10th, 50th, and 90th percentiles of residual noise of the 4100 ft-A station accumulated over the course of two months. The filter is either updated once a day, leading to the dashed-line percentiles, or once per week leading to the solid-line percentiles. The filter order was 1000 calculated from 2 hours of data. The subtraction performance is almost identical in the two cases, which means that seismic correlations averaged over one day do not change significantly within one week. It is in fact remarkable that the residual spectra are so similar over a wide range of frequencies. It is to be expected though that this result would look differently if the Wiener filter is instead applied to channels of a complex system such as a laser interferometer.

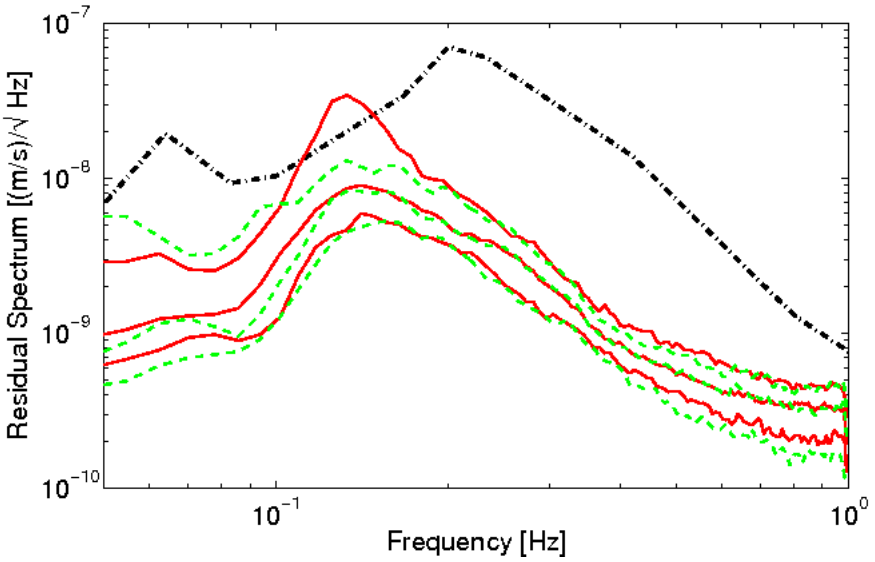

FIG. 3: Plot comparing subtraction residuals over a month of data. The dashed curves are its 10th, 50th, and 90th percentiles using a filter that is updated once every day. The solid lines are the percentiles of residual noise using a filter updated once every week.

.

B. Optimal filter order

When designing and optimizing a Wiener filter, there are only a few tunable parameters. This includes the number of reference channels that one uses to create the filter, as well as what kind of additional filtering (if any) to apply to the input data. Another is the order of the Wiener FIR filter. Implementations in GW interferometers [6–8] have typically used thousands of filter coefficients at 64 Hz sampling rate. These filters were calculated using 1 hour of data.

One may wonder whether the order of the most efficient Wiener filter, i. e. the filter with minimal order achieving the subtraction goal, only depends on the bandwidth of the noise that one wants to subtract. This assumption seems reasonable, because the filter order and time interval between two filter coefficients determines the minimum and maximum frequency of the filter response. It will be shown in this section that the dependence of subtraction residuals on filter order is not so simple.

We examine the effect of filter order using three separate days of data. For each day, filters are calculated with varying filter order. In figure 4, the performances of the filters are

compared. The plot on the left shows the noise reduction at 0.12 Hz (arbitrarily chosen) for the three days and filter orders 1 to 1000, while the plot on the right is the same for 0.2 Hz. Filter order 1 means simple subtraction of data with optimal scaling factor of the input data. Subtraction performance shows less variation from one day to the next for high filter orders,

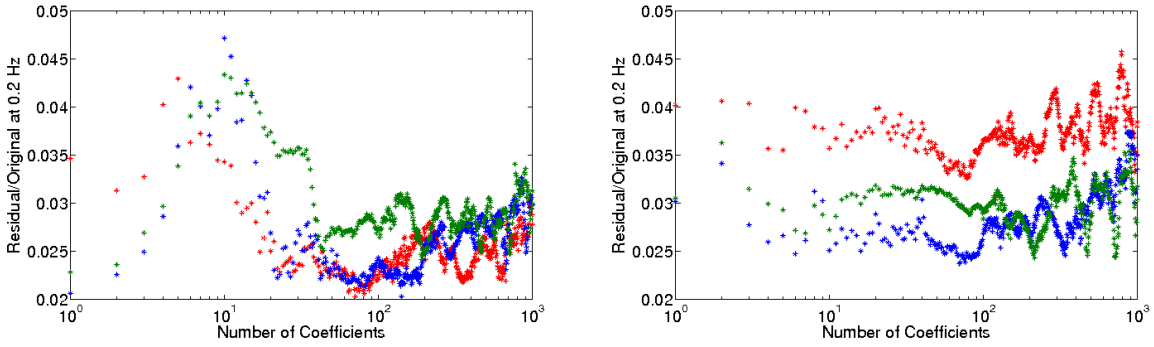

FIG. 4: Residual noise evaluated over the three separate days as a function of filter order. The residuals shown in the plot on the left are evaluated at 0.12 Hz, whereas the residuals on the right are evaluated at 0.2 Hz.

but the price paid for this stability is that the residuals could be much less at certain days using a smaller filter order. In general, best subtraction performance is only achieved for specific filter orders, often degraded substantially when changing from optimal filter order to slightly higher or smaller orders. In addition, the optimal filter order is not the same every day. However, the plots also show that even though choosing the optimal filter order depends on target frequency and varies between days, it is still possible to identify ranges of filter order that work better than others. For example, for the two frequencies 0.12 Hz and 0.2 Hz, figure 4 shows that a filter order slightly below 100 would be a better choice instead of a very high filter order around 1000.

A full histogram of residuals achieved for the day represented by the blue markers in figure 4 accumulated from all filter orders between 1 and 1000 is shown in figure 5. Even though dependence of the residuals on filter order seems modest at most frequencies, it should be emphasized that even a factor 1.5 in residual noise can be significant especially with respect to NN, which directly contributes to the detection band.

These results suggest that an adaptive filter technology that includes modifications of the filter order could lead to significantly decreased residuals. At least in the case of NN cancellation, which does not necessarily have to be carried out in real time, it is also conceivable

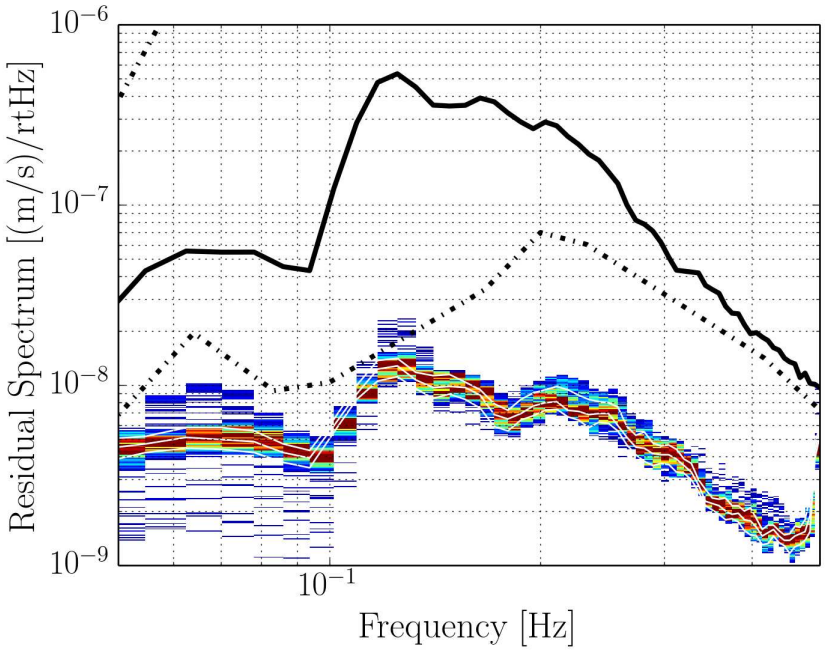

FIG. 5: The plot shows the histogram of residual spectra achieved by each of the 1000 filter orders for the day represented by the blue markers in figure 4.

to apply a sequence of Wiener filters with different orders.

V. CONCLUSION

As shown in various publications in the past, Wiener filters can be used to efficiently subtract noise from data off-line, or in real time by means of feed-forward noise cancellation. In this paper, we focused on subtraction of coherent seismic noise, but many other applications are conceivable and have already been applied in previous generations of GW detectors often forming an important part of the detector design. Wiener filters can subtract broadband noise as well as narrow-band features such as noise lines, and they will therefore play an important role in future detectors, and also serve as a starting point for the development of more advanced filter technologies.

In this paper, we have demonstrated that we can achieve more than an order of magnitude noise cancellation between about 0.05-0.5 Hz using Wiener filters with only a few seismometers separated by a distance of order 500 m. We have also shown that this subtrac-

tion performance can be achieved without regularly updating the filter, indicating that the average properties of seismic fields do not change significantly over timescales of weeks in this frequency band. However, in the attempt to optimize noise cancellation, it was found that filter order plays an important role. At frequencies below 0.1 Hz, subtraction residuals varied almost by an order of magnitude for filter orders between $1 - 1000$. Whereas continuous optimization of filter order may not be feasible in many applications, especially in system control, the results also show that there are ranges of filter order with near-optimal subtraction performance over a broader range of frequencies. These filter orders maintain near-optimal performance over days.

Because the residual spectra also contain a microseismic peak, it is evident that noise cancellation is not only limited by instrumental noise. A theory that should be tested in the future is whether the residual peak is produced by body waves instead of surface waves. It is known that both wave types contribute to the microseisms, but it is not clear how this affects noise cancellation. Alternatively, it is possible that topographic scattering of seismic waves play a role. The Homestake seismic underground array will be expanded in the future to more seismometers. This will make it possible to carry out a number of important studies relevant to seismic-noise cancellation, which were impossible with the array used here. The extended array will have the capabilities to distinguish between body and surface waves, which, as explained, will be important to explore and possibly understand seismic-noise cancellation limits.

VI. ACKNOWLEDGMENTS

MC was supported by the National Science Foundation Graduate Research Fellowship Program, under NSF grant number DGE 1144152. VD is a member of the LIGO Laboratory, supported by funding from United States National Science Foundation. NC's work was supported by NSF grant PHY-1204371. LIGO was constructed by the California Institute of Technology and Massachusetts Institute of Technology with funding from the National Science Foundation and operates under cooperative agreement PHY-0757058. This paper has been assigned LIGO document number ligo-p1400042.

References

[1] G. M. Harry and the LIGO Scientific Collaboration, Classical and Quantum Gravity **27**, 084006 (2010), URL http://stacks.iop.org/0264-9381/27/i=8/a=084006.

[2] T. Accadia, F. Acernese, F. Antonucci, P. Astone, G. Ballardin, F. Barone, M. Barsuglia, A. Basti, T. S. Bauer, M. Bebronne, et al., Classical and Quantum Gravity **28**, 114002 (2011).

[3] K. Somiya, Classical and Quantum Gravity **29**, 124007 (2012).

[4] M. Punturo, M. Abernathy, F. Acernese, B. Allen, N. Andersson, K. Arun, F. Barone, B. Barr, M. Barsuglia, M. Beker, et al., Classical and Quantum Gravity **27**, 194002 (2010).

[5] R. Abbott, R. Adhikari, G. Allen, D. Baglino, C. Campbell, D. Coyne, E. Daw, D. DeBra, J. Faludi, P. Fritschel, et al., Classical and Quantum Gravity **21**, S915 (2004), URL http://stacks.iop.org/0264-9381/21/i=5/a=081.

[6] J. A. Giaime, E. J. Daw, M. Weitz, R. Adhikari, P. Fritschel, R. Abbott, R. Bork, and J. Heefner, Review of Scientific Instruments **74** (2003).

[7] J. Driggers, M. Evans, K. Pepper, and R. Adhikari, Review of Scientific Instruments **83**, 024501 (2012).

[8] R. DeRosa, J. C. Driggers, D. Atkinson, H. Miao, V. Frolov, M. Landry, J. A. Giaime, and R. X. Adhikari, Classical and Quantum Gravity **29**, 215008 (2012), URL http://stacks.iop.org/0264-9381/29/i=21/a=215008.

[9] P. R. Saulson, Phys. Rev. D **30**, 732 (1984).

[10] S. A. Hughes and K. S. Thorne, Phys. Rev. D **58**, 122002 (1998).

[11] T. Creighton, Class. Quantum Grav. **25**, 125011 (2008).

[12] M. Beker, G. Cella, R. DeSalvo, M. Doets, H. Grote, J. Harms, E. Hennes, V. Mandic, D. Rabeling, J. van den Brand, et al., General Relativity and Gravitation **43**, 623 (2011).

[13] J. Harms, F. Acernese, F. Barone, I. Bartos, M. Beker, J. van den Brand, N. Christensen, M. Coughlin, R. DeSalvo, S. Dorsher, et al., Classical and Quantum Gravity **27**, 225011 (2010).

[14] G. Cella, in *Recent Developments in General Relativity* (Springer, 2000), pp. 495–503.

[15] J. C. Driggers, J. Harms, and R. X. Adhikari, Phys. Rev. D **86**, 102001 (2012), URL http:

//link.aps.org/doi/10.1103/PhysRevD.86.102001.

[16] S. V. Vaseghi, *Wiener Filters* (John Wiley & Sons, Ltd, 2001), pp. 178–204, ISBN 9780470841624.

[17] A. H. Sayed, *Fundamentals of Adaptive Filtering* (John Wiley & Sons, 2003).

[18] Wang J., Tilmann F. J., White R. S., Soosalu H., and Bordoni P., Leading Edge **27**, 232 (2008).

[19] M. Coughlin, the Ligo Scientific Collaboration, and the Virgo Collaboration, Journal of Physics: Conference Series **243**, 012010 (2010), URL http://stacks.iop.org/1742-6596/243/i=1/a=012010.

[20] M. W. Coughlin, for the LIGO Scientific Collaboration, and the Virgo Collaboration, Classical and Quantum Gravity **28**, 235008 (2011), URL http://stacks.iop.org/0264-9381/28/i=23/a=235008.

[21] N. Christensen, the LIGO Scientific Collaboration, and the Virgo Collaboration, Classical and Quantum Gravity **27**, 194010 (2010), URL http://stacks.iop.org/0264-9381/27/i=19/a=194010.

[22] T. Isogai, the Ligo Scientific Collaboration, and the Virgo Collaboration, Journal of Physics: Conference Series **243**, 012005 (2010), URL http://stacks.iop.org/1742-6596/243/i=1/a=012005.

[23] G. D. Meadors, K. Kawabe, and K. Riles, arXiv preprint arXiv:1311.6835 (2013).

[24] B. Allen, W. Hua, and A. Ottewill, arXiv preprint gr-qc/9909083 (1999).

[25] K. Kokeyama, K. Izumi, W. Z. Korth, N. Smith-Lefebvre, K. Arai, and R. X. Adhikari, J. Opt. Soc. Am. A **31**, 81 (2014), URL http://josaa.osa.org/abstract.cfm?URI=josaa-31-1-81.

[26] M. Coughlin and J. Harms, Classical and Quantum Gravity **29**, 075004 (2012), URL http://stacks.iop.org/0264-9381/29/i=7/a=075004.

[27] J. Peterson, Open-file report **93-322** (1993).